bioRxiv preprint doi: https://doi.org/10.1101/2023.12.01.569666; this version posted December 2, 2023. The copyright holder for this preprint (which was not certified by peer review) is the author/funder, who has granted bioRxiv a license to display the preprint in perpetuity. It is made available under aCC-BY-NC-ND 4.0 International license.

Intracellular Ebola Virus nucleocapsid assembly revealed by *in situ* cryo-electron tomography.

Reika Watanabe[1], Dawid Zyla[1], Diptiben Parekh[1], Connor Hong[1], Ying Jones[2], Sharon L. Schendel[1], Willian Wan[3], Guillaume Castillon[2] and Erica Ollmann Saphire[1,4]*

[1]La Jolla Institute for Immunology, La Jolla, CA USA
[2]Electron Microscopy Core, University of California San Diego, La Jolla, CA USA
[3]Vanderbilt University Center for Structural Biology, Nashville, TN
[4]Dept. of Medicine, University of California San Diego, La Jolla, CA 92037
*Corresponding author

Abstract

Filoviruses, including Ebola and Marburg viruses, are a family of highly lethal viruses that cause severe hemorrhagic fever in humans with near annual outbreaks. Antiviral options are limited, and broad-spectrum antivirals are needed. The core of the filamentous virion is formed by the nucleocapsid, a helical structure in which the polymerized nucleoprotein (NP) assembles on the RNA genome and is surrounded by viral proteins VP24 and VP35[1,2]. The mechanism by which these proteins assemble to form nucleocapsids inside infected cells is unclear, and the identity of the outer half of nucleocapsid density remains unassigned. Using cryo-electron tomography, we revealed the assembly process of Ebola virus in both cells transfected with the viral proteins and cells infected with a biologically contained model Ebola virus. We obtained a fully assembled intracellular nucleocapsid-like structure at 9 Å that allows assignment of previously unassigned densities and presents the first complete model of the intracellular Ebola nucleocapsid. Our model reveals a previously unknown, third layer of additional copies of NP in complex with VP35. In this outer layer, the N-terminal domain of VP35 maintains NP in a monomeric form, and the rest of VP35 appears to participate in an intra-rung nucleocapsid interaction. The C-terminal region of NP lies outside this third outer layer, allowing localization and recruitment of additional viral proteins and connection of the nucleocapsid to the matrix beneath the virus envelope. Comparison of this in-cell nucleocapsid to previous in-virion structures reveals that the nucleocapsid helix condenses upon incorporation into the virion. Molecular interfaces responsible for nucleocapsid assembly are conserved among filoviruses, offering potential target sites for broadly effective antivirals. The architecture and assembly dynamics of Ebola virus nucleocapsids revealed here uncover a unique filovirus nucleocapsid assembly and a condensation mechanism that protect viral genome integrity in the virion.

Main text

Filoviruses, including Ebola and Marburg viruses, are a family of highly lethal viruses that cause severe hemorrhagic fever in humans[3]. Filoviruses are in the order Mononegavirales, which includes multiple pathogenic human viruses such as rabies, measles, and respiratory syncytial viruses. Mononegavirales are enveloped viruses with a non-segmented, single-stranded negative-

bioRxiv preprint doi: https://doi.org/10.1101/2023.12.01.569666; this version posted December 2, 2023. The copyright holder for this preprint (which was not certified by peer review) is the author/funder, who has granted bioRxiv a license to display the preprint in perpetuity. It is made available under aCC-BY-NC-ND 4.0 International license.

sense RNA genome that is encapsulated by nucleoprotein (NP) to form a helical nucleocapsid. In filoviruses, two other viral proteins, VP35 and VP24, are also required to form the nucleocapsid [4,5]. Binding of VP35 to nascent NP is thought to prevent oligomerization of NP before binding to the viral RNA genome[6–10]. VP35 also functions as an essential virus RNA polymerase cofactor, linking the viral polymerase with the genome-NP template[11–13]. VP24 is unique to the filovirus family. In addition to its critical role in nucleocapsid formation, VP24 regulates viral transcription and replication[14] and intracellular transport of the nucleocapsid [15]. Importantly, VP35 and VP24 also suppress host immune signaling, influencing viral replication and pathogenicity [16–21]. Prior work revealed nucleocapsid-like structures in budded viruses or virus-like-particles [1,2]. In these structures, a repeating unit of the nucleocapsid consists of two adjacent copies of core NP molecules that polymerizes along the viral genome, plus two VP24 molecules[2]. The N-terminal half of NP was visible, but the location and structure of both the C-terminal half of NP and the essential VP35 protein remained unknown. It was also unknown why in the pair of VP24 molecules, every other copy was positioned in the opposite orientation. Further, until recently, it was impossible to reveal protein structures directly inside cells. Therefore, we had no structural insights into how Ebola virus replicates and nucleocapsids assemble in infected cells prior to budding and release.

Intracellular Ebola virus nucleocapsid assembly and structures

To elucidate the nucleocapsid assembly process, we first used HEK293T cells transfected with complete EBOV NP or NP lacking C-terminal amino acids 601-739 (NPΔ601-739), in combination with VP24 and VP35 (Extended Data Fig. 1a). NPΔ601-739 was selected for analysis as it is the shortest NP known to form a fully assembled nucleocapsid [22]. We expected that comparing two nucleocapsid structures with full-length or C-terminal truncated NP would help identify the previously unassigned C-terminal domain of NP [2] in the intracellular nucleocapsid structure. During viral replication in the cell cytoplasm, nucleocapsid assembly exclusively occurs inside viral replication factories, also known as viral inclusion bodies [23,24]. These structures exclude most host cellular organelles, and have heterogeneous size and morphology (Extended Data Fig. 1h, i). Immunofluorescence microscopy confirms that all transfected proteins (NP, VP35, and VP24) co-localize into these replication factories (Extended Data Fig. 1b-g). Resin-embedded, ultra-thin section, transmission electron microscopy shows that in the presence of VP24 and VP35, both NP and NPΔ601-739 efficiently form bundles of electron-dense, assembled, intracellular nucleocapsid-like structures inside the replication factories (Extended Data Fig. 1h, i).

To gain structural insight into the nucleocapsid assembly process, we investigated the transfected cells using cryo-electron tomography coupled with focused ion beam milling[25]. We identified three distinct intracellular nucleocapsid precursors: loosely coiled NP polymers, regionally condensed NP polymers, and fully assembled nucleocapsid-like structures (Extended Data Fig. 2a-g). We determined nucleocapsid coordinates by cylinder correlation, and performed the first subtomogram averaging to resolve their overall structures (Extended Data Fig. 3, 4). We found that all intracellular nucleocapsid-like structures (whether from complete NP or C-

bioRxiv preprint doi: https://doi.org/10.1101/2023.12.01.569666; this version posted December 2, 2023. The copyright holder for this preprint (which was not certified by peer review) is the author/funder, who has granted bioRxiv a license to display the preprint in perpetuity. It is made available under aCC-BY-NC-ND 4.0 International license.

terminally truncated NP) form a left-handed helix with a diameter of 52 nm and nearly identical helical parameters (Fig. 1a, 2a).

To obtain higher resolution structures of individual repeating units that form these helical structures, we performed further subtomogram analysis by re-extracting subtomograms, and centering their repeating units based on the helical parameters (Extended Data Fig. 3, 4). We performed 3D classification and 3D refinement without applying any helical symmetry, considering the highly heterogeneous nature of filovirus nucleocapsid structures in virions[1,2,26] (Extended Data Fig. 3, 4). We obtained 9 Å and 18 Å resolution maps of intracellular nucleocapsid structures in cells expressing C-terminally truncated NPΔ601-739 and full-length NP, respectively (Fig. 1b-d,k, 2b,c, Extended Data Fig. 3, 4). These structures have overall similarity to previous nucleocapsid structures observed in viral-like-particles and Ebola virions[2] (Fig. 3). Our 9 Å map shows the highest local resolution in the central repeating unit (Fig.1k). By combining this map with pre-existing high-resolution structures, we could build an atomic model of the intracellular nucleocapsid structure (Fig. 1e-h, Extended Data Fig. 5).

Within a single repeating unit (colored in Fig. 1b-d), we assigned two NP core domains (NP^{core}#1 in blue, NP^{core}#2 in cyan) and two VP24 molecules (VP24 #1in purple, VP24 #2 in pink). Together this pair of RNA-bound NPs and their antiparallel VP24s (one up and one down) form the same repeating unit as observed using budded virus or virus-like-particles[2] (Fig. 1e-h).

Based on the outer layers of our map (Fig. 1k) that had higher local resolution than previous structures[2] (Extended data Fig. 5a see EM map resolution), we could, for the first time, interpret previously unassigned outer density of the nucleocapsid. We observed and definitively assigned the position of a third copy of NP on the outer layer in a region beyond the previously visualized central NP-RNA helix (Fig. 1e-h). This newly-assigned NP (NP^{core}#3 in green) is not bound to the viral genome, but instead localizes to the outer layer attached to VP24#2 (previously identified as inverted relative to VP24#1, but not known why; Fig. 1e-h). Serial docking of the newly assigned outer NP density with pre-existing x-ray/cryoEM structures showed the best in-map density correlation with a crystal structure of NP in complex with the N-terminal NP-binding peptide of VP35[10]. This NP-binding peptide of VP35 holds NP in a monomeric state[10,27] and is unambiguously recognizable in our EM map (Fig. 1i,j). This interaction of VP35 with nascent NP is thought to prevent oligomerization of NP and is a mechanism that is widely conserved among Mononegavirales[6–10].

We also assigned density in the outer layer of the nucleocapsid for the C-terminal domain of VP35 ($VP35^{CTD}$, amino acids 215-340, orange in Fig. 1e-h). Based on this $VP35^{CTD}$ location, we could fit the crystal structure of VP35 amino acids 81-340, the longest VP35 structure experimentally modeled[13,28]. In the nucleocapsid visualized here, the central oligomerization domain of VP35 (aa 80-145) points toward NP^{core}#3 of the adjacent repeating unit (Fig. 1l-n). Although we could not clearly visualize density associated with the VP35 oligomerization domain in our map[13,28], in part due to its higher flexibility relative to its C-terminal domain, the directional angle of this domain toward the adjacent NP^{core}#3 further supports the model in which an outer layer of NP is complexed with VP35 (Fig. 1l-n). This bridge-like conformation of the extended

bioRxiv preprint doi: https://doi.org/10.1101/2023.12.01.569666; this version posted December 2, 2023. The copyright holder for this preprint (which was not certified by peer review) is the author/funder, who has granted bioRxiv a license to display the preprint in perpetuity. It is made available under aCC-BY-NC-ND 4.0 International license.

VP35 molecule suggests that the outer NP^{core}#3 takes part in an intra-rung nucleocapsid interaction via interaction with VP35. Our finding is consistent with the fact that VP35 is specifically required to form the layer of nucleocapsid outside the core NP^{NTD}-RNA helix [4,5], and the first example among Mononegavirales of a nucleoprotein that also functions in a monomeric form in the nucleocapsid.

In virus assembly, NP binds to the matrix protein VP40 and drives incorporation of the nucleocapsid into the virion [29,30]. However, the NP-RNA central helix is surrounded by a thick VP24 layer that is estimated to be around 7 nm wide (Fig 1c-h). This thick VP24 layer could hinder direct interaction of NP, contained in the central NP-RNA helix, with matrix proteins outside. VP24 is known to play a role in host immune evasion [16–19,31] and thus carrying sufficient copies of VP24 as part of the payload of the entering nucleocapsid could benefit the virus by limiting host immune responses from the earliest time points after infection. Incorporating an additional, monomeric form of NP in the outermost layer of the nucleocapsid could sterically facilitate the needed NP-VP40 matrix interactions despite the VP24 coating layer.

C-terminal regions of NP are located between intracellular nucleocapsids.

We found that our two in-cell nucleocapsid-like structures, one for full-length NP and the other for C-terminally truncated NPΔ601-739, are essentially identical, except in resolution (9 Å vs. 18 Å; Fig. 1a,b vs Fig. 2a,b and Extended data Fig. 3j,k and 4j,k). Our 9 Å atomic model for C-terminally truncated NP fits well into the 18 Å map of the intracellular nucleocapsid-like structure with full-length NP (Fig. 2d-f), and we used this fitting to locate the NP C-terminal domain. The first hint of its location came from observing how intracellular nucleocapsids are aligned and bundled within virus replication factories in cells. The intracellular nucleocapsid for full-length NP has greater inter-nucleocapsid spatial separation between parallel nucleocapsids than do bundled nucleocapsids formed by NPΔ601-739 (Fig. 2g,h,j,k): 14 nm for full-length NP vs. 2 nm for NPΔ601-739. These values are based on center-to-center distances of coordinates obtained from filament tracing (Fig. 2i,l). Considering the location of the C-terminal end of NP^{core}#3 on outer layer of the nucleocapsid and the critical role of NP CTD for interactions with matrix proteins[29,30], we propose that the NP CTD, together with the rest of the intrinsically disordered domain of NP (aa 601-644) occupies the space between the nucleocapsid and the nucleocapsid-matrix in the virion (Fig. 2f). This gap is consistently 7 nm wide on either side of the 52 nm-wide nucleocapsid (Fig. 2f,g, and 4k).

Ebola virus nucleocapsids are further tightened upon incorporation into virions.

In previous studies of in-virion Ebola virus nucleocapsids, outer density was present but could not be assigned (Fig. 3a,b,d,e)[2]. Docking of our in-cell nucleocapsid atomic model into density of the prior in-virion nucleocapsid in virus-like particles (EMDB:3871)[2] and flexible refinement yielded a more complete model of the Ebola nucleocapsid in virions (Fig 3c, Extended Data Fig. 5). We also evaluated the inverse process wherein we docked our in-virion nucleocapsid model into the

bioRxiv preprint doi: https://doi.org/10.1101/2023.12.01.569666; this version posted December 2, 2023. The copyright holder for this preprint (which was not certified by peer review) is the author/funder, who has granted bioRxiv a license to display the preprint in perpetuity. It is made available under aCC-BY-NC-ND 4.0 International license.

density of the in-virion Ebola virus nucleocapsid (Fig 3f). In virions, density for the VP35 CTD is very weak, suggesting that this position is rarely fully or stably occupied in the virus[2].

Although the single repeating units are almost identical between in-cell and in-virion structures (RMSD 1.07 Å estimated with backbone C-alpha trace; Fig. 3g), the inter-rung and intra-rung associations differ between in-cell and in-virion models (Fig. 3h-n) and EM maps (Extended Data Fig. 6a-j). The helical pitches of intracellular nucleocapsids obtained here (85 Å and 87 Å for full-length NP and Δ601-739NP, respectively) are consistently larger than those previously reported for in-virion nucleocapsids[2] (75 Å and 74 Å for budded virus-like particles and budded authentic Ebola virus, respectively). We also revealed a longer inter-rung gap for in-cell nucleocapsids compared to in-virion nucleocapsids, which is consistent with the different pitches (Fig. 3k,l Extended Data Fig. 6g-j, red and cyan triangles). The final budded nucleocapsids in the virions are thus more condensed than their intracellular pre-budded nucleocapsid counterparts. Interestingly, in our 3D classification of intracellular nucleocapsids, some regions exhibit shorter inter-rung distances even within the same particles. These regions that have narrower inter-rung distances lack the outer NP-VP35 complex (Extended Data Fig. 7, class 1, 6, and 7 highlighted in red arrowhead). Together, these findings suggest that the outer NP-VP35 complex bridges interactions between adjacent repeating units and may determine some optimal distance. Upon incorporation into virus particles, the nucleocapsid vertically condenses [Fig. 4k (iii) to (iv)]. This condensation protects RNA genome integrity through tight NP-inter-rung associations mediated by electrostatic interactions[2,32]. The interaction of the outer NP C-terminal domain with matrix protein on the viral envelope likely triggers this further nucleocapsid condensation.

EBOV-GFP-ΔVP30-infected cells illuminate the nucleocapsid assembly process in the context of viral infection.

Next, we visualized the nucleocapsid assembly process in the context of viral infection, rather than in transfected cells. To operate outside BSL-4 containment, we used a biologically contained model Ebola virus, EBOV-GFP-ΔVP30 (Fig. 4, Extended Data Fig. 8). In this model, the gene encoding VP30, which is essential for viral transcription, is replaced in the viral genome by a gene encoding green fluorescence protein (GFP). EBOV-GFP-ΔVP30 virions can enter cells, but can not replicate unless VP30 is supplied in trans[33]. The GFP reporter indicates the presence of viral replication activity in infected cells (Extended Data Fig. 8a,b). In EBOV-GFP-ΔVP30-infected cells, similar to authentic virus infection, NP is assembled on the viral RNA genome in the presence of all viral proteins, which, except for VP30, are all expressed under intrinsic control from the viral genome [33]. VP30 is expressed by an exogenous promoter in the stable cell lines [33]. In this system, both virus and infected cells are operable outside a BSL-4 environment [34].

Using cryo-electron tomography coupled with cryo-fluorescence microscopy and focused-ion beam milling of plunge-frozen EBOV-GFP-ΔVP30-infected cells, we observed intracellular virus replication 24 hours post-infection (Fig. 4 a-e and Extended data Fig. 8c-e). The morphology of virus replication factories in these infected cells is similar to that observed in cells transfected

bioRxiv preprint doi: https://doi.org/10.1101/2023.12.01.569666; this version posted December 2, 2023. The copyright holder for this preprint (which was not certified by peer review) is the author/funder, who has granted bioRxiv a license to display the preprint in perpetuity. It is made available under aCC-BY-NC-ND 4.0 International license.

with NP, VP24, and VP35 (Extended data Fig 2a). Most host cytoplasmic organelles, such as mitochondria, membrane structures, and cytoskeleton, are excluded from the virus replication factory (Fig. 4 a,b, Extended Data Fig. 8d), which is filled with loosely coiled NP-RNA complexes and fully assembled nucleocapsid structures (Fig. 4c, d). One difference between nucleocapsid structures from transfected and infected cells is that in the transfected cells, we also observe regionally condensed nucleocapsid structures (Extended data Fig. 2c, d) whereas in virus-infected cells, only loose or fully condensed structures, rather than regionally condensed intermediates, are visible. In viral infection, NP binds VP30, preferentially associates with the viral RNA genome, and recruits RNA-dependent RNA polymerase L through interaction with VP35, to facilitate RNA genome replication and viral mRNA transcription[35]. We suspect that all these activities prevent the spontaneous regional condensation of NP seen in transfected cells (Extended data Fig. 2c, d). In virus-infected cells, recruitment and physical binding of VP24, VP35, and outer NP are required to condense the NP helix and this condensation is required to shift the transcriptionally active, more open nucleocapsid into its inactive condensed structure before incorporation into virion [Fig. 4k (i) to (ii)].

In several tomograms of intracellular nucleocapsids in infected cells, we saw additional visible density protruding from the nucleocapsid (Fig. 4e, highlighted with blue arrowheads). These protrusions likely correspond to the C-terminal regions of NP (601-739) that protrude from the well-resolved nucleocapsid (Fig. 2f) to associate with other viral proteins like VP30, polymerase L, and VP40 [Fig. 4k (iii)]. Immunofluorescence microscopy of VP30 and VP40 localized in viral replication factories supports this possibility (Extended data Fig. 8f, g). Based on our atomic model of the in-cell nucleocapsid combined with the recently revealed structure of the Ebola virus polymerase L-VP35 complex [13,28], we speculate that polymerase L is localized on the external side of the nucleocapsid, where it is recruited by interaction with VP35 complexed with the outer NP^{core}#3 (Fig. 4j). Interestingly, in the Ebola virus nucleocapsid, the density of the VP35 C-terminal domain is not fully occupied (Fig. 3d-f). We speculate that the association between polymerase L and VP35 destabilizes the VP24-VP35 interaction (VP24#1 and $VP35^{CTD}$ shown in Fig. 3c) freeing the polymerase L-VP35 complex to swing out from the nucleocapsid, thus resulting in low occupancy of $VP35^{CTD}$ in the virion (Fig. 3d-f). Further, the polymerase L-VP35 complex associates with nucleocapsid via the outer NP for incorporation of the polymerase complex into the virion payload.

We also visualized assembled EBOV-GFP-ΔVP30 virions emerging from the infected cell, by imaging the cell periphery of frozen-hydrated EBOV-GFP-ΔVP30-infected cells using cryo-electron-tomography combined with cryo-fluorescence microscopy (Fig. 4f-i, Extended data Fig. 8h,i). In these emerging virions, the viral nucleocapsid lies at the center of the filamentous virion, surrounded by VP40 matrix proteins (Fig. 4f-h). The existence of some hypothetical flexible linker-like structure, of unknown identity, connecting the nucleocapsid to the matrix has been proposed to help position the nucleocapsid in the center of the virion and to minimize nucleocapsid breakage when the long filamentous viruses bend [36]. The in-virion nucleocapsid in EBOV-GFP-ΔVP30 viruses is also surrounded by structures similar to that of the intracellular nucleocapsid.

bioRxiv preprint doi: https://doi.org/10.1101/2023.12.01.569666; this version posted December 2, 2023. The copyright holder for this preprint (which was not certified by peer review) is the author/funder, who has granted bioRxiv a license to display the preprint in perpetuity. It is made available under aCC-BY-NC-ND 4.0 International license.

Such structures of the budded nucleocapsids are particularly visible in particles that have lost the surrounding membrane envelope (Fig. 4i). These observations support the idea that in infected cells, the NP C-terminal region (aa 601-739) recruits other viral proteins to the nucleocapsids and functions as a flexible linker between the nucleocapsid and matrix proteins in the virion [Fig. 4k (iv)] to protect viral genome integrity. In the tomographic slice shown in Fig. 4f, the matrix-to-matrix distance in virion is roughly 66 nm, which matches well with the predicated 66 nm width of the entire nucleocapsid including the NP C-terminal domain [Fig. 2f and Fig. 4k (iv)].

Conserved inter-molecular interfaces in filovirus nucleocapsid assembly

Our atomic model of an intracellular nucleocapsid revealed at least six interfaces within the repeating unit, plus two additional interfaces that form inter-rung or intra-rung surfaces between adjacent repeating units (Fig. 5, Extended Data Table1). At the current 9 Å resolution of our EM map, we can identify protein regions, but not the individual contact amino acids involved in each interface. Each of these interfaces is described in the order protein A-protein B in which protein A is toward the nucleocapsid interior, while protein B is toward the nucleocapsid exterior.

The following features characterize the different interfaces: **(i)** The interface between NP#1 and NP#2 localized in the central NP-RNA helix, is mediated by insertion of the N-terminal helix (aa 20-37, red) of NP#1 into the pockets of the adjacent NP#2 that are formed by aa 247-258 and 281-296 [yellow; (Fig. 5a)]. This interface is identical to that observed in assembled recombinant NP N-terminal domain (1-450) and in nucleocapsids of budded virions [2,32]; **(ii)** The interface between $VP35^{N\text{-}termBP}$ and NP^{core} of NP#3, on the outer layer of the nucleocapsid, is mediated by an interaction between the N-terminal NP-binding peptide of VP35 (NP interaction site is aa 27-45 of VP35 in blue, bracketed by aa 21-26 and 46-50 of VP35 in orange) with the C-terminal lobe of the NP core (aa 245-254 plus 274-291 of NP, yellow; Fig. 5b) and is identical to that seen in crystal structures[10,27]. Superimposing NP#2 and NP#3 demonstrates that the N-terminal helix of NP#1 and the N-terminal NP-binding peptide of VP35 both insert into the same NP pocket, NP#1 into this pocket of NP#2, and $VP35^{N\text{-}termBP}$ into this pocket of NP#3, indicating a single NP can bind only one of these potential nucleocapsid binding partners at a time. We also note that arrangements of several α helices in the C-lobe differ between NP#2 and NP#3 (Fig. 5c). We conclude that the different layers of NP assembled in the nucleocapsid are tuned to perform two distinct functions. One function, achieved by NP#1 and NP#2 together on the inside, is to polymerize and bind RNA to form the central NP-RNA helix and protect the viral genome. The other function involves NP#3 on the outside, interacting in a monomeric form with matrix proteins, to drive nucleocapsid incorporation into the virion; **(iii)** The interface of NP#1-VP24#1 is mainly mediated by two loops of the NP (aa 60-65 and 189-196, yellow; Fig. 5d) and two loops of VP24 (aa 108-112 and 143-153, red; Fig. 5d). **(iv)** Interestingly, roughly the same interfaces are used by the interaction of VP24#2 (aa 109-113, 143-149, red) with the outer NP#3 (aa 61-66, 194-206, yellow). Superimposing NP#1-VP24#1 and VP24#2-NP#3 shows an almost perfect match between the VP24 and N-lobe of NP, demonstrating that the same VP24 and NP interaction occurs at two different locations within the repeating unit, one facing inward and the other facing outward

bioRxiv preprint doi: https://doi.org/10.1101/2023.12.01.569666; this version posted December 2, 2023. The copyright holder for this preprint (which was not certified by peer review) is the author/funder, who has granted bioRxiv a license to display the preprint in perpetuity. It is made available under aCC-BY-NC-ND 4.0 International license.

in the nucleocapsid (Fig. 5f). **(v)** In the interface between NP#2 and VP24#2, a VP24 loop that includes aa 53-68 (red; Fig. 5g) interacts with two NP loops (aa 61-64, 189-198; yellow Fig. 5g). Superimposing the NP#1-VP24#1 and NP#2-VP24#2 complexes reveals that nearly identical NP surfaces are involved in interactions, but the two bound VP24 are in opposite orientations (Fig. 5h). **(vi)** The interface of VP24#1-VP35^{CTD} is mediated by loops from VP24 (aa 170-175, red; Fig. 5i) and VP35 (aa 330-334, blue; Fig. 5i). Superimposing NP#2-VP24#2 and VP24#1-VP35^{CTD} complexes reveals that VP35^{CTD} and NP bind to the same side of VP24: the binding of VP35^{CTD} to VP24#1 overlaps with the binding of NP#2 to VP24#2 (Fig. 5j). The overlap of binding suggests that binding of VP35^{CTD} to VP24#1 prevents a second NP from binding this VP24#1. **(vii)** The interface between VP24#1 with an NP#3 on the next rung down (yellow box, Fig. 5k) mediates the inter-rung interactions that build the intracellular nucleocapsid. This inter-rung interaction is mediated by a VP24 helix (aa 67-74, red) and an NP loop (aa 181-184, yellow; Fig. 5l). Alanine substitution of aa 73-77 of VP24 abrogates NP binding in co-immunoprecipitation experiments performed in the absence of VP35[14], providing biochemical evidence for this newly visualized VP24#1-inter-rung NP#3 interface (interface vii).

We find that inter-rung distances differ significantly between in-cell and in-virion nucleocapsids (Fig. 3h-l, Extended Data Fig. 6), with in-cell nucleocapsids being more open, and in-virion nucleocapsids being more condensed. A side-to-side comparison of the corresponding regions reveals that the inter-rung interface (vii) in-cell nucleocapsid (Fig. 3m, yellow arrowhead) is not present in the in-virion nucleocapsid. Further, the potential inter-rung interface identified in the in-virion nucleocapsid between VP24#1 and NP#3 on the next rung down is shifted upward (Fig. 3n red arrowhead). At the resolution of the map around this area of the in-virion nucleocapsid (EMDB-3871), we cannot define the presence or identity of potential inter-rung interactions in the virion.

(viii) The final interface is a hypothetical interface between NP#3 and VP35 that is predicted by fitting the VP35 crystal structure (aa 80-340) into the clear density corresponding to residues 221-340 of VP35^{CTD} (Fig. 1k-m, Fig. 5k,m highlighted by a red box). In addition to the known NP-binding peptide of VP35 that interacts with the second lobe of the NP core (c-lobe), as visualized in the interface (ii) (VP35 aa 27-45 blue; Fig. 5b) and crystal structures[10], the oligomerization domain of VP35 (aa 81-112) likely interacts with NP as well (Fig. 5m). This possibility is supported by the finding that in biochemical assays, VP35 (aa 80-120) contains an NP binding site that is independent of the NP binding by the VP35 N terminus (aa 1-80) [10]. Together with interface (ii), we speculate that interface (viii) functions to maintain intra-rung interactions of the outer nucleocapsid structure. Notably, to our knowledge, all NP interfaces that interact with VP24 are in the structurally stable, first, N-terminal lobe of the NP core (aa 15-240). In contrast, VP35-interacting sites are located in the rest of NP (aa 240-600), as observed here and identified in biochemical studies[14,37,38]. Although we did not model the intrinsically disordered C-terminal region of NP (aa 405-600), due to its flexibility and current resolution of our EM map, this region of NP (aa 451-600) is critical for nucleocapsid formation in the presence of VP24 and VP35[22]. A higher-resolution map will be needed to understand details of these interaction sites.

bioRxiv preprint doi: https://doi.org/10.1101/2023.12.01.569666; this version posted December 2, 2023. The copyright holder for this preprint (which was not certified by peer review) is the author/funder, who has granted bioRxiv a license to display the preprint in perpetuity. It is made available under aCC-BY-NC-ND 4.0 International license.

We found that the regions comprising the seven visualized interfaces (i to vii) are well-conserved among six different filoviruses (Extended data Fig. 9). The interface viii was not included in this analysis since we currently cannot determine precise interacting regions. After sequence alignment with T-Coffee, we calculated the average conservation score of these interface regions using three different metrics [39–41] and compared the regions to scores for the full-length proteins (Extended Data Table 1). All three metrics indicated that the conservation scores for all the interface regions are substantially higher than the average score for the full-length proteins, suggesting that nucleocapsid assembly architecture and the interfaces are likely conserved across different filoviruses (Extended Data Fig. 10). The architecture and assembly dynamics of EBOV nucleocapsids revealed here uncover the unique, but well-conserved nature of filovirus nucleocapsid assembly and pave the way to develop broadly applicable antivirals.

In summary, the intracellular nucleocapsid structures presented here reveal a previously unknown third layer of the nucleocapsid, which includes NP maintained in a monomeric, genome-free state by VP35, as well as the likely location of the NP C-terminal domain, deduced by visualization of how nucleocapsids bundle in transfected cells and how the single nucleocapsid lies in the virion. Our intracellular structures also reveal the distinct intermolecular interactions between the separate copies of NP and VP24 and that the distinct copies of the NP molecule play different roles in the assembly. Further, the study reveals structural differences between in-virion and in-cell nucleocapsids, with a more open structure in-cell, and additional inter-rung interactions only visible in-cell, revealing how the viral nucleocapsid condenses vertically as the nucleocapsid matures and transits from the replication factory to its final budded virion. The conserved interfaces revealed in the nucleocapsid assembly provide new directions for antiviral development, and new template for basic research exploration of viral function.

bioRxiv preprint doi: https://doi.org/10.1101/2023.12.01.569666; this version posted December 2, 2023. The copyright holder for this preprint (which was not certified by peer review) is the author/funder, who has granted bioRxiv a license to display the preprint in perpetuity. It is made available under aCC-BY-NC-ND 4.0 International license.

Fig. 1: Structure of intracellular Ebola NPΔ601-739-VP24-VP35 nucleocapsid.

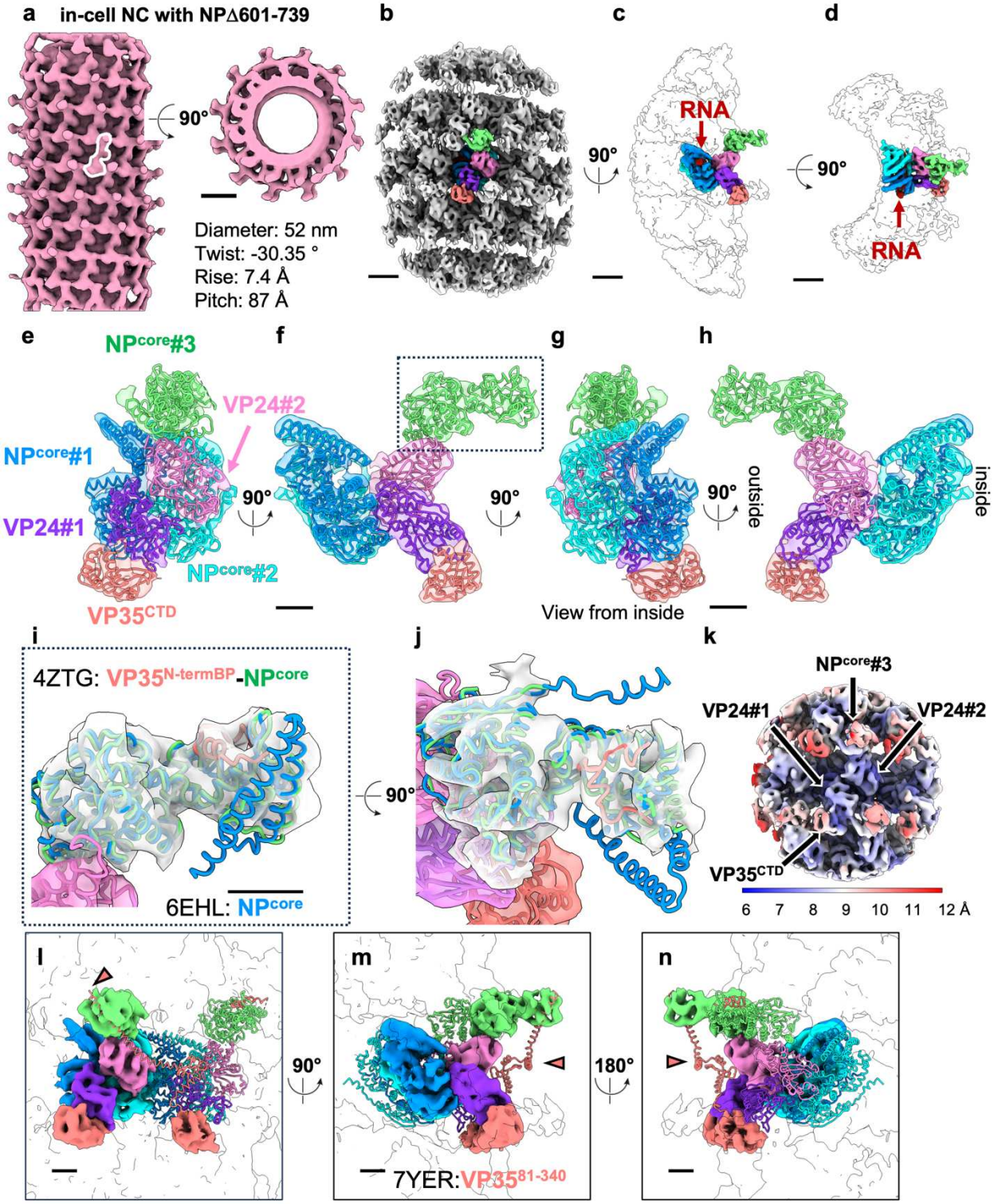

bioRxiv preprint doi: https://doi.org/10.1101/2023.12.01.569666; this version posted December 2, 2023. The copyright holder for this preprint (which was not certified by peer review) is the author/funder, who has granted bioRxiv a license to display the preprint in perpetuity. It is made available under aCC-BY-NC-ND 4.0 International license.

Fig. 1: Structure of intracellular Ebola NPΔ601-739-VP24-VP35 nucleocapsid.

a, The initial map of intracellular Ebola NPΔ601-739-VP24-VP35 nucleocapsid (pink) shows a left-handed helix with helical parameters as indicated. The repeating unit is marked with a white outline. **b-d**, Intracellular NPΔ601-739-VP24-VP35 nucleocapsid subunit densities. The two central NP core domains (NP^{core}#1, NP^{core}#2) are in blue and cyan. Two copies of VP24 (VP24#1, VP24#2) are in purple and pink. The C-terminal domain of VP35 ($VP35^{CTD}$) is in orange and the third NP core (NP^{core}#3) is in green. Continuous red density at the interior core of the NP copies corresponds to RNA (Also shown in Extended Data Fig. 5b). **e-h**, Molecular models fitted into EM densities. Colors are as in b-d. **i** and **j,** Crystal structure of NP complexed with the VP35 N-terminal NP-binding peptide (green and orange; PDB:4ZTG)[10] and the NP core model built into the in-virion nucleocapsid (blue; PDB:6EHL)[2] each fitted into the outermost density indicated by the dotted line in f. The specific density corresponding to the VP35 N-terminal binding peptide from 4ZTG (orange), is visible in the densities. Within NP^{core} model (6EHL in blue) , N-terminal helix (aa 16-37) involved in NP^{core}-polymerization, region including the part of penultimate helix (aa 359-366) and clamp helix (aa 370-405) involved in RNA clamping[2], clearly locate outside of density. **k,** Local resolution map showing the highest resolution in the central repeating unit. **l-n**, Molecular models of VP35 (aa 81-340)(PDB:7YER)[13] fitted into the $VP35^{CTD}$ density. Scale bars indicate 10 nm (**a**), 5 nm (**b-d**), 2 nm (**f, h, i, j, l-n**)

bioRxiv preprint doi: https://doi.org/10.1101/2023.12.01.569666; this version posted December 2, 2023. The copyright holder for this preprint (which was not certified by peer review) is the author/funder, who has granted bioRxiv a license to display the preprint in perpetuity. It is made available under aCC-BY-NC-ND 4.0 International license.

Fig. 2: Structure of intracellular Ebola NP-VP24-VP35 from full-length NP.

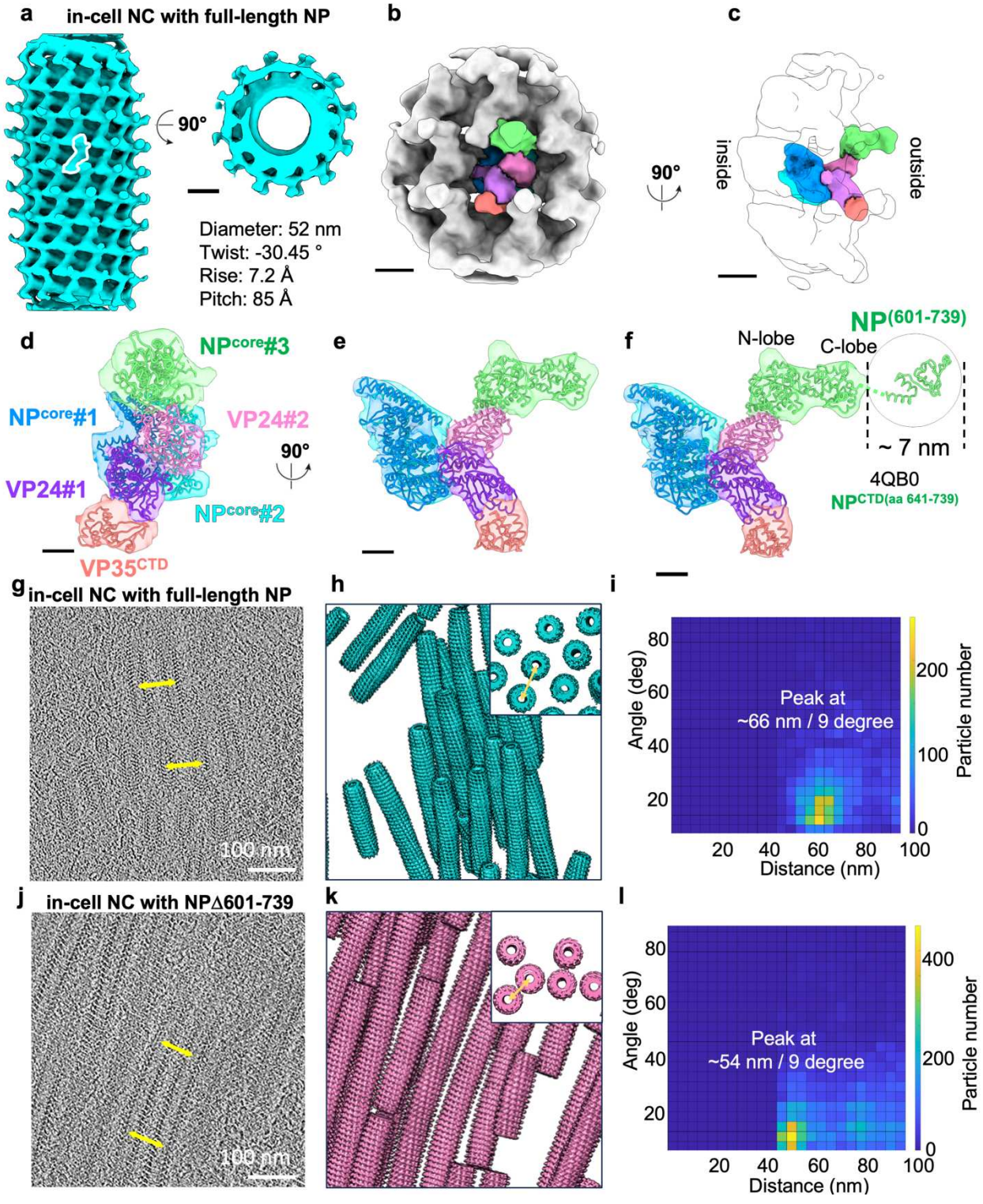

bioRxiv preprint doi: https://doi.org/10.1101/2023.12.01.569666; this version posted December 2, 2023. The copyright holder for this preprint (which was not certified by peer review) is the author/funder, who has granted bioRxiv a license to display the preprint in perpetuity. It is made available under aCC-BY-NC-ND 4.0 International license.

Fig. 2: Structure of intracellular Ebola NP-VP24-VP35 from full-length NP.

a, Initial map of the intracellular Ebola virus nucleocapsid made from full-length NP-VP24-VP35 showing a left-handed helix with helical parameters as indicated. The repeating unit is marked with a white outline. **b-c**, Intracellular full-length NP-VP24-VP35 nucleocapsid subunit densities. The two central NP core domains (NP^{core}#1, NP^{core}#2) are in blue and cyan. Two VP24 molecules (VP24#1, VP24#2) are in purple and pink. The C-terminal domain of VP35 ($VP35^{CTD}$) is in orange and the third NP core (NP^{core}#3) is in green. **d-f**, Molecular models fitted into the EM densities and the hypothetical position of NP aa 601-739 based on the measured distance between intracellular nucleocapsids. The crystal structure of the NP C-terminal domain (aa 641-739; PDB:4QB0)[42] is fit into the gap. **g and j**, Representative tomographic slices of cells, **h and k**, Initial averages mapped back onto tomograms, and **i and l**, Two-dimensional histograms showing the distance of the center-to-center and angle of the intracellular nucleocapsids formed by full-length NP-VP24-VP35 and NPΔ601-739-VP24-VP35, respectively. Yellow lines in **g, h, j** and **k** indicate the center-to-center distance of the closest neighboring nucleocapsid. **h** and **k** panel insets show oriented views to visualize the distance between aligned nucleocapsids. Scale bars indicate 10 nm (**a**), 5 nm (**b-c**), 2 nm (**d-f**), 100 nm (**g, j**).

bioRxiv preprint doi: https://doi.org/10.1101/2023.12.01.569666; this version posted December 2, 2023. The copyright holder for this preprint (which was not certified by peer review) is the author/funder, who has granted bioRxiv a license to display the preprint in perpetuity. It is made available under aCC-BY-NC-ND 4.0 International license.

Fig. 3: Molecular model of in-virion nucleocapsids and further condensation of intracellular nucleocapsid upon virion incorporation.

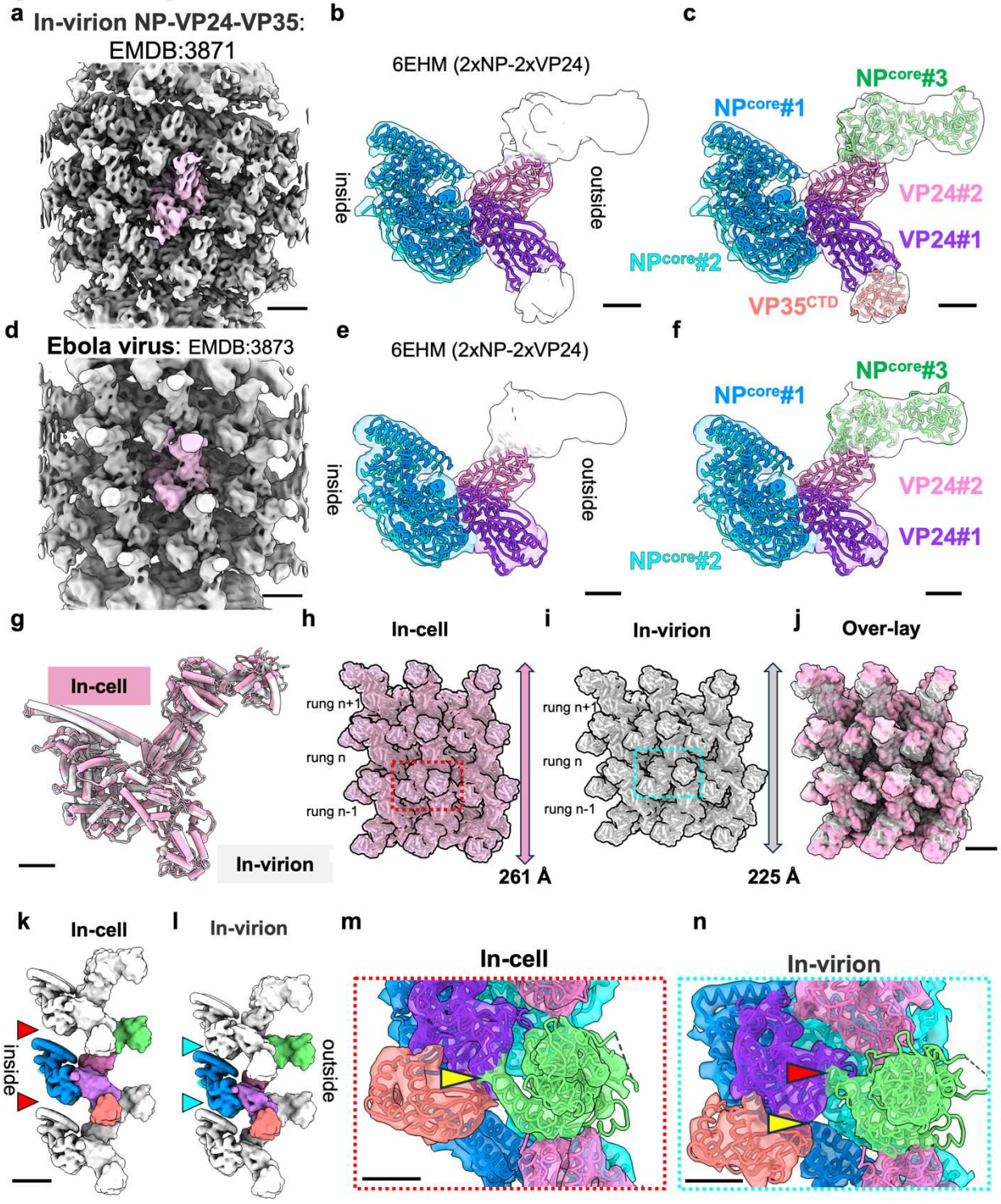

bioRxiv preprint doi: https://doi.org/10.1101/2023.12.01.569666; this version posted December 2, 2023. The copyright holder for this preprint (which was not certified by peer review) is the author/funder, who has granted bioRxiv a license to display the preprint in perpetuity. It is made available under aCC-BY-NC-ND 4.0 International license.

Fig. 3: Molecular model of in-virion nucleocapsids and further condensation of intracellular nucleocapsid upon virion incorporation.

a, and **d**, Visualization of in-virion NP-VP24-VP35 (EMDB: 3871) and Ebola nucleocapsid (EMDB:3873), respectively[2]. The single repeating units are highlighted in pink. **b** and **e**, EM densities fitted with the molecular model of two copies of NP (in blue and cyan) and two copies of VP24 (in purple and pink) (PDB: 6EHM) molecules show previously unannotated densities (white)[2]. **c** and **f**, In-virion model created based on an in-cell model (Figures 1 and 2) fitted into EM densities of the authentic virus. Model colors correspond to those for Fig. 1e. **g**, Comparison of single repeating units of intracellular (in-cell) and in-virion nucleocapsid shows that the models are nearly identical (RMSD 1.07 Å). **h-j**, Assembled models consisting of nine repeating units of intracellular and in-virion nucleocapsid models based on intracellular NP(Δ601-739)-VP24-VP35 and in-virion NP-VP24-VP35 nucleocapsid densities and their overlaid models. In the overlaid model, in-cell surface density is shown in opaque pink. **k and l**, Side view of assembled models consisting of three vertically aligned nucleocapsid models based on EM densities of intracellular NPΔ601-739-VP24-VP35 and in-virion NP-VP24-VP35 (EMDB: 3871) nucleocapsids, respectively. Red and blue arrowheads show wider and narrower inter-rung spaces, respectively. **m** and **n,** Enlarged views of the boxed regions in h and i. The inter-rung interface identified in the in-cell nucleocapsid (yellow arrowhead in **m**) is not present in the in-virion nucleocapsid (**n**). Further, the potential inter-rung interface in the in-virion nucleocapsid is shifted upward (red arrowhead). In n, yellow arrowhead points to the same location of VP24 (purple) as in m as a reference point. Molecular models are fitted into the EM densities. Inter-rung interaction sites within the two repeating units differ between intracellular and in-virion nucleocapsids. Scale bars indicate 5 nm (**a,d, j,k**) and 2 nm (**b, c, e, f, g, m, n**).

bioRxiv preprint doi: https://doi.org/10.1101/2023.12.01.569666; this version posted December 2, 2023. The copyright holder for this preprint (which was not certified by peer review) is the author/funder, who has granted bioRxiv a license to display the preprint in perpetuity. It is made available under aCC-BY-NC-ND 4.0 International license.

Fig. 4: EBOV-GFP-ΔVP30 virus-infected cells illuminate the authentic assembly process

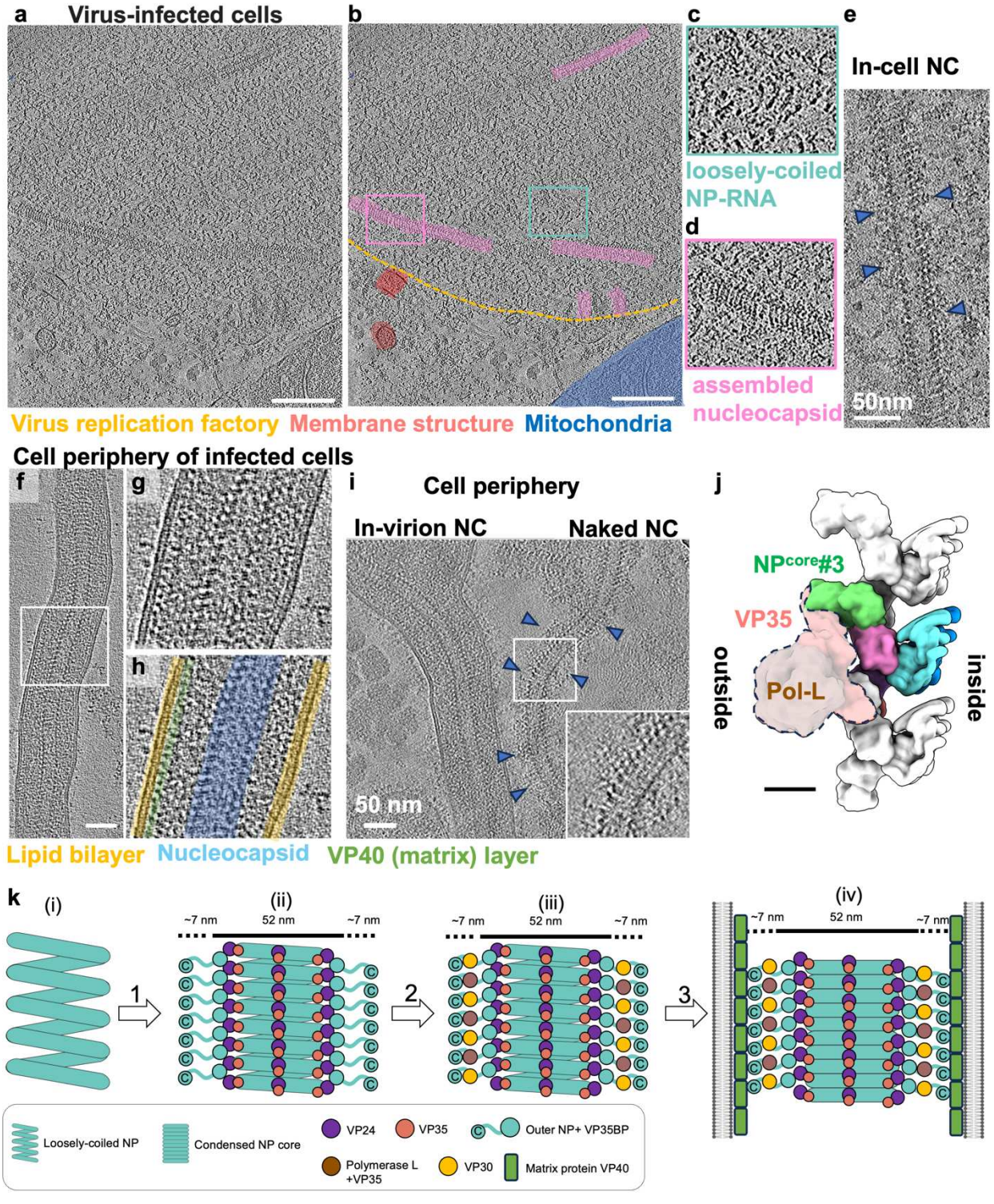

bioRxiv preprint doi: https://doi.org/10.1101/2023.12.01.569666; this version posted December 2, 2023. The copyright holder for this preprint (which was not certified by peer review) is the author/funder, who has granted bioRxiv a license to display the preprint in perpetuity. It is made available under aCC-BY-NC-ND 4.0 International license.

Fig. 4: EBOV-GFP-ΔVP30 virus-infected cells illuminate the authentic assembly process
a, Representative tomographic slice of FIB-milled EBOV-GFP-ΔVP30 virus-infected cells frozen 24 hours post-infection. Panel **b** shows annotation of the tomogram in a. The replication factory is inside and above the yellow curve. Assembled Ebola virus nucleocapsids are highlighted in pink. Host membrane structures are orange and mitochondria blue. **c** and **d,** Enlarged views of the boxed regions in b. The area outlined in cyan contains loosely coiled NP-RNA. **e**, Representative tomographic slice showing intracellular nucleocapsid found in EBOV-GFP-ΔVP30 virus-infected cells. Blue arrowheads indicate fluffy densities extending from the intracellular nucleocapsid. **f,** Representative tomographic slice of a virus emerging from frozen EBOV-GFP-ΔVP30 infected cells 24 hours post-infection. **g**, Enlarged view of the boxed region in f. **h**, Annotation of tomogram in g. The viral envelope lipid bilayer, matrix protein, VP40 layer, and nucleocapsids are in yellow, green, and blue, respectively. **i,** Representative tomographic slice of intact virus and naked nucleocapsids without viral envelope found in the cell periphery of frozen infected cells 24 hours post-infection. Blue arrowheads highlight fluffy densities extending from the in-virion nucleocapsid. Inset: Enlarged views of the boxed region. **j**, Model of polymerase L complexed with VP35[13] fitted with our intracellular nucleocapsids. **k**, Schematic representation of the Ebola virus nucleocapsid assembly process described in this study. (i) The loosely coiled nucleocapsids represent transcription and replication-competent NP assembly bound to viral RNA genome and viral polymerase L via VP35. (ii) When enough viral proteins accumulate in viral factories, VP24, VP35, and outer NP assemble on the loosely coiled nucleocapsids, which transition into a rigid and condensed state. A portion of the intrinsically disordered domain and C-terminal domain of NP extends from the assembled nucleocapsid and fills the additional 7 nm-wide space along the intracellular nucleocapsid. (iii) In addition to the three major nucleocapsid protein components, the essential transcription factor VP30, polymerase L, and a matrix protein VP40 are recruited to nucleocapsids for incorporation into the virion and formation of fully functional nucleocapsids competent to propagate infection. Both VP30 and VP40 bind to the extended region of NP [29,30,43,44]. (iv) Assembled nucleocapsid is incorporated into virions through interactions between the NP C-terminal domain and matrix protein that lies beneath the viral envelope. In the virion, nucleocapsids are further condensed relative to intracellular nucleocapsids to ensure genome integrity. In the virion, the intrinsically disordered domain and CTD of NP functions as a flexible linker that positions the nucleocapsid at the center of the virion. This link may also confer a certain amount of flexibility to minimize genome breakage in case of membrane deformation. The matrix-to-matrix distance in the virion measured in the tomographic slice shown in **f-h** is ~66 nm, which matches well with the estimated width of ~66 nm of nucleocapsid including NP (aa 601-739) regions (52 + 14 nm) shown in Fig. 2 **f**. Scale bars indicate 200 nm (**a**,**b**), 50 nm (**e,f,i**), and 5 nm (**j**).

bioRxiv preprint doi: https://doi.org/10.1101/2023.12.01.569666; this version posted December 2, 2023. The copyright holder for this preprint (which was not certified by peer review) is the author/funder, who has granted bioRxiv a license to display the preprint in perpetuity. It is made available under aCC-BY-NC-ND 4.0 International license.

Fig. 5: Interfaces involved in nucleocapsid formation

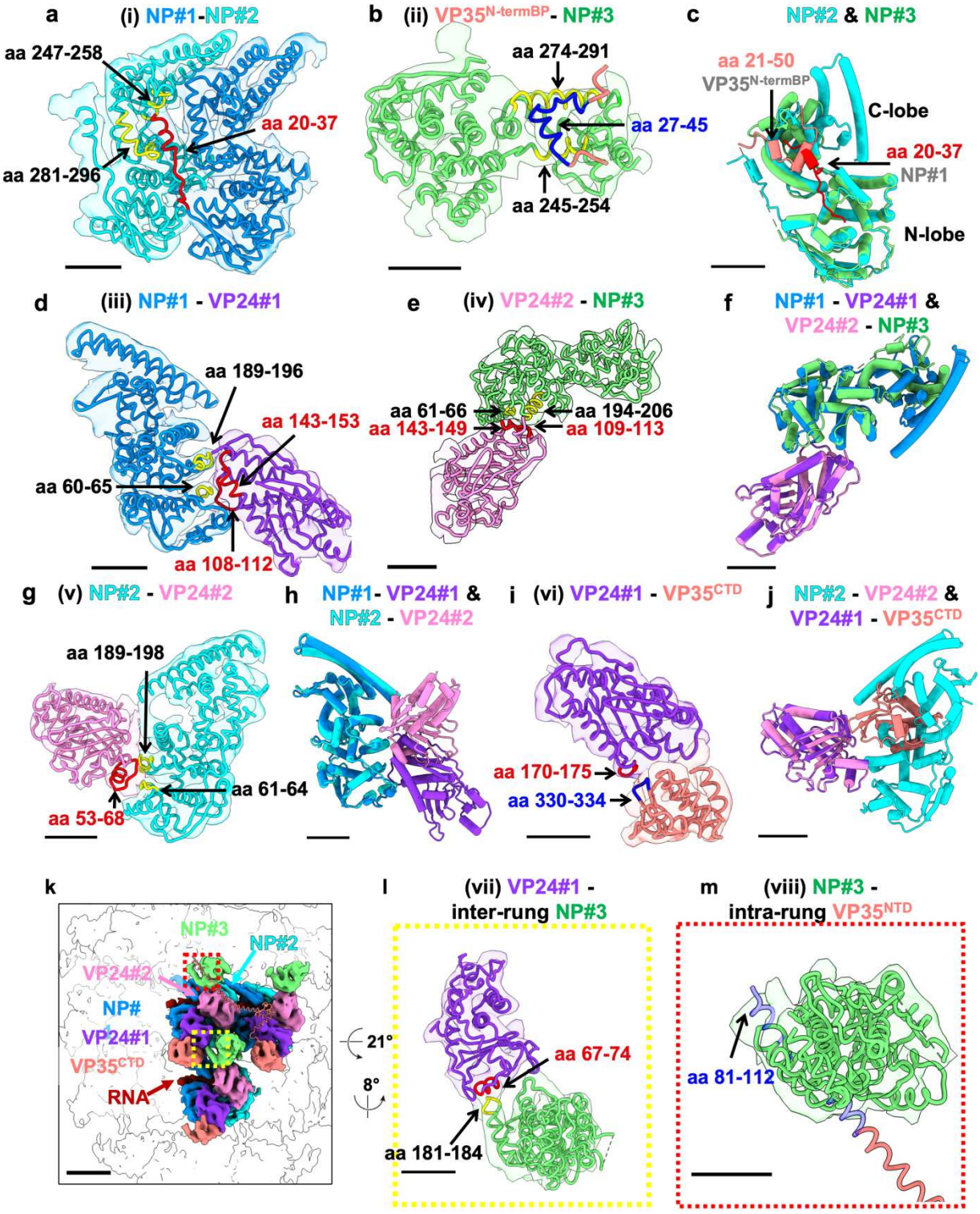

bioRxiv preprint doi: https://doi.org/10.1101/2023.12.01.569666; this version posted December 2, 2023. The copyright holder for this preprint (which was not certified by peer review) is the author/funder, who has granted bioRxiv a license to display the preprint in perpetuity. It is made available under aCC-BY-NC-ND 4.0 International license.

Fig. 5: Interfaces involved in nucleocapsid formation

a, Interface (i) NP#1-NP#2. The view is from inside the nucleocapsid as shown in Fig. 1g. **b**, Interface (ii) VP35$^{\text{N-termBP}}$-NP$^{\text{core}}$. The view is from the top of the nucleocapsid as shown in Fig. 1j. **c,** Superimposing NP#2 and NP#3 focusing on the overlapping locations of the N-terminal tail from the adjacent NP (red), VP35 N-terminal binding peptide (orange) and conformational changes in the NP C-terminal lobe between the two structures that results in flexibility and lack of clear density for C-lobe helices in the green NP#3. **d**, Interface (iii) NP#1-VP24#1. Side view as shown in Fig. 1f. **e**, Interface (iv) VP24#2-NP#3. Side view as shown in Fig. 1f. **f**, Superimposing NP#1-VP24#1 and VP24#2-NP#3 with alignment of the VP24#1 and VP24#2 shows an almost perfect fit of VP24 and the NP N-terminal lobe, confirming that the same VP24 and NP interaction occurs in two different locations within the repeating unit. **g**, Interface (v) NP#2-VP24#2. Side view as shown in Fig. 1h. **h**, Superimposing NP#1-VP24#1 and NP#2-VP24#2 with alignment of NP#1 and NP#2 reveals that almost the same NP surfaces are involved in interaction with VP24 in two different orientations. **i**, Interface (vi) VP24#1-VP35$^{\text{CTD}}$. Side view as shown in Fig. 1f. **j**, Superimposing NP#2-VP24#2 and VP24#1-VP35$^{\text{CTD}}$ with alignment of VP24#2 and VP24#1 reveals that VP35 binding to VP24 prevents binding of a second NP to VP24#1. **k**, Three central repeating units are colored within the EM density of intracellular NPΔ601-739-VP24-VP35. The VP35 structure (aa 81-340)[13] is fitted in one of VP35$^{\text{CTD}}$ densities (orange). Yellow and red boxes show inter-rung and intra-rung interfaces, respectively. **l**, Interface (vii) VP24#1-inter-rung NP#3. **m**, Hypothetical interface (viii) NP#3 -intra-rung VP35$^{\text{NTD}}$ predicted by fitting the VP35 structure (aa 81-340) at the location of adjacent VP35$^{\text{CTD}}$. Predicted density corresponding to VP35$^{\text{NTD}}$ obtained from the model was not observed, likely due to the flexibility of the VP35 oligomerization domains that would change the helix angles. We estimate that VP35 (aa 81 to 112 highlighted by transparent blue) could potentially interact with NP#3 (aa 241 to 600). (**a**-**m**), The color of each fit model matches that of the EM map in other figures. Regions forming interfaces are colored yellow, red, and blue to distinguish them from the rest of the proteins. Density thresholds are set to show helical densities. Amino acid sequences involved in the interfaces are listed in Extended Data Table 1. Scale bars indicate 2 nm except in **k**; 5nm.

bioRxiv preprint doi: https://doi.org/10.1101/2023.12.01.569666; this version posted December 2, 2023. The copyright holder for this preprint (which was not certified by peer review) is the author/funder, who has granted bioRxiv a license to display the preprint in perpetuity. It is made available under aCC-BY-NC-ND 4.0 International license.

References

1. Bharat TAM, Noda T, Riches JD, Kraehling V, Kolesnikova L, Becker S, Kawaoka Y, Briggs JAG. Structural dissection of Ebola virus and its assembly determinants using cryo-electron tomography. Proc Natl Acad Sci U S A. 2012 Mar 13;109(11):4275–4280. PMCID: PMC3306676

2. Wan W, Kolesnikova L, Clarke M, Koehler A, Noda T, Becker S, Briggs JAG. Structure and assembly of the Ebola virus nucleocapsid. Nature. 2017 Nov 16;551(7680):394–397. PMCID: PMC5714281

3. Malvy D, McElroy AK, de Clerck H, Günther S, van Griensven J. Ebola virus disease. Lancet. 2019 Mar 2;393(10174):936–948. PMID: 30777297

4. Noda T, Ebihara H, Muramoto Y, Fujii K, Takada A, Sagara H, Kim JH, Kida H, Feldmann H, Kawaoka Y. Assembly and budding of Ebolavirus. PLoS Pathog. 2006 Sep;2(9):e99. PMCID: PMC1579243

5. Huang Y, Xu L, Sun Y, Nabel GJ. The assembly of Ebola virus nucleocapsid requires virion-associated proteins 35 and 24 and posttranslational modification of nucleoprotein. Mol Cell. 2002 Aug;10(2):307–316. PMID: 12191476

6. Curran J, Marq JB, Kolakofsky D. An N-terminal domain of the Sendai paramyxovirus P protein acts as a chaperone for the NP protein during the nascent chain assembly step of genome replication. J Virol. 1995 Feb;69(2):849–855. PMCID: PMC188651

7. Majumdar A, Bhattacharya R, Basak S, Shaila MS, Chattopadhyay D, Roy S. P-protein of Chandipura virus is an N-protein-specific chaperone that acts at the nucleation stage. Biochemistry. 2004 Mar 16;43(10):2863–2870. PMID: 15005621

8. Leyrat C, Yabukarski F, Tarbouriech N, Ribeiro EA Jr, Jensen MR, Blackledge M, Ruigrok RWH, Jamin M. Structure of the vesicular stomatitis virus N^0-P complex. PLoS Pathog. 2011 Sep;7(9):e1002248. PMCID: PMC3178552

9. Yabukarski F, Lawrence P, Tarbouriech N, Bourhis JM, Delaforge E, Jensen MR, Ruigrok RWH, Blackledge M, Volchkov V, Jamin M. Structure of Nipah virus unassembled nucleoprotein in complex with its viral chaperone. Nat Struct Mol Biol. 2014 Sep;21(9):754–759. PMID: 25108352

10. Kirchdoerfer RN, Abelson DM, Li S, Wood MR, Saphire EO. Assembly of the Ebola Virus Nucleoprotein from a Chaperoned VP35 Complex. Cell Rep. 2015 Jul 7;12(1):140–149. PMCID: PMC4500542

11. Mühlberger E, Weik M, Volchkov VE, Klenk HD, Becker S. Comparison of the transcription and replication strategies of marburg virus and Ebola virus by using artificial replication systems. J Virol. 1999 Mar;73(3):2333–2342. PMCID: PMC104478

12. Shu T, Gan T, Bai P, Wang X, Qian Q, Zhou H, Cheng Q, Qiu Y, Yin L, Zhong J, Zhou X.

bioRxiv preprint doi: https://doi.org/10.1101/2023.12.01.569666; this version posted December 2, 2023. The copyright holder for this preprint (which was not certified by peer review) is the author/funder, who has granted bioRxiv a license to display the preprint in perpetuity. It is made available under aCC-BY-NC-ND 4.0 International license.

Ebola virus VP35 has novel NTPase and helicase-like activities. Nucleic Acids Res. 2019 Jun 20;47(11):5837–5851. PMCID: PMC6582406

13. Yuan B, Peng Q, Cheng J, Wang M, Zhong J, Qi J, Gao GF, Shi Y. Structure of the Ebola virus polymerase complex. Nature. 2022 Oct;610(7931):394–401. PMCID: PMC9517992

14. Banadyga L, Hoenen T, Ambroggio X, Dunham E, Groseth A, Ebihara H. Ebola virus VP24 interacts with NP to facilitate nucleocapsid assembly and genome packaging. Sci Rep. 2017 Aug 9;7(1):7698.

15. Takamatsu Y, Kolesnikova L, Becker S. Ebola virus proteins NP, VP35, and VP24 are essential and sufficient to mediate nucleocapsid transport. Proc Natl Acad Sci U S A. 2018 Jan 30;115(5):1075–1080. PMCID: PMC5798334

16. Zhang APP, Bornholdt ZA, Liu T, Abelson DM, Lee DE, Li S, Woods VL Jr, Saphire EO. The ebola virus interferon antagonist VP24 directly binds STAT1 and has a novel, pyramidal fold. PLoS Pathog. 2012 Feb;8(2):e1002550. PMCID: PMC3285596

17. Xu W, Edwards MR, Borek DM, Feagins AR, Mittal A, Alinger JB, Berry KN, Yen B, Hamilton J, Brett TJ, Pappu RV, Leung DW, Basler CF, Amarasinghe GK. Ebola virus VP24 targets a unique NLS binding site on karyopherin alpha 5 to selectively compete with nuclear import of phosphorylated STAT1. Cell Host Microbe. 2014 Aug 13;16(2):187–200. PMCID: PMC4188415

18. Mateo M, Reid SP, Leung LW, Basler CF, Volchkov VE. Ebolavirus VP24 binding to karyopherins is required for inhibition of interferon signaling. J Virol. 2010 Jan;84(2):1169–1175. PMCID: PMC2798383

19. Messaoudi I, Amarasinghe GK, Basler CF. Filovirus pathogenesis and immune evasion: insights from Ebola virus and Marburg virus. Nat Rev Microbiol. 2015 Nov;13(11):663–676. PMCID: PMC5201123

20. Kimberlin CR, Bornholdt ZA, Li S, Woods VL, MacRae IJ, Saphire EO. *Ebolavirus* VP35 uses a bimodal strategy to bind dsRNA for innate immune suppression [Internet]. Proceedings of the National Academy of Sciences. 2010. p. 314–319. Available from: http://dx.doi.org/10.1073/pnas.0910547107

21. Cárdenas WB, Loo YM, Gale M Jr, Hartman AL, Kimberlin CR, Martínez-Sobrido L, Saphire EO, Basler CF. Ebola virus VP35 protein binds double-stranded RNA and inhibits alpha/beta interferon production induced by RIG-I signaling. J Virol. 2006 Jun;80(11):5168–5178. PMCID: PMC1472134

22. Watanabe S, Noda T, Kawaoka Y. Functional mapping of the nucleoprotein of Ebola virus. J Virol. 2006 Apr;80(8):3743–3751. PMCID: PMC1440433

23. Hoenen T, Shabman RS, Groseth A, Herwig A, Weber M, Schudt G, Dolnik O, Basler CF, Becker S, Feldmann H. Inclusion bodies are a site of ebolavirus replication. J Virol. 2012 Nov;86(21):11779–11788. PMCID: PMC3486333

bioRxiv preprint doi: https://doi.org/10.1101/2023.12.01.569666; this version posted December 2, 2023. The copyright holder for this preprint (which was not certified by peer review) is the author/funder, who has granted bioRxiv a license to display the preprint in perpetuity. It is made available under aCC-BY-NC-ND 4.0 International license.

24. Geisbert TW, Jahrling PB. Differentiation of filoviruses by electron microscopy. Virus Res. 1995 Dec;39(2-3):129–150. PMID: 8837880

25. Wagner FR, Watanabe R, Schampers R, Singh D, Persoon H, Schaffer M, Fruhstorfer P, Plitzko J, Villa E. Preparing samples from whole cells using focused-ion-beam milling for cryo-electron tomography. Nat Protoc. 2020 Jun;15(6):2041–2070. PMID: 32405053

26. Bharat TAM, Riches JD, Kolesnikova L, Welsch S, Krähling V, Davey N, Parsy ML, Becker S, Briggs JAG. Cryo-electron tomography of Marburg virus particles and their morphogenesis within infected cells. PLoS Biol. 2011 Nov;9(11):e1001196. PMCID: PMC3217011

27. Leung DW, Borek D, Luthra P, Binning JM, Anantpadma M, Liu G, Harvey IB, Su Z, Endlich-Frazier A, Pan J, Shabman RS, Chiu W, Davey RA, Otwinowski Z, Basler CF, Amarasinghe GK. An Intrinsically Disordered Peptide from Ebola Virus VP35 Controls Viral RNA Synthesis by Modulating Nucleoprotein-RNA Interactions. Cell Rep. 2015 Apr 21;11(3):376–389. PMCID: PMC4599368

28. Peng Q, Yuan B, Cheng J, Wang M, Gao S, Bai S, Zhao X, Qi J, Gao GF, Shi Y. Molecular mechanism of de novo replication by the Ebola virus polymerase. Nature [Internet]. 2023 Sep 12; Available from: http://dx.doi.org/10.1038/s41586-023-06608-1 PMID: 37699521

29. Noda T, Watanabe S, Sagara H, Kawaoka Y. Mapping of the VP40-binding regions of the nucleoprotein of Ebola virus. J Virol. 2007 Apr;81(7):3554–3562. PMCID: PMC1866061

30. Licata Jillian M., Johnson Reed F., Han Ziying, Harty Ronald N. Contribution of Ebola Virus Glycoprotein, Nucleoprotein, and VP24 to Budding of VP40 Virus-Like Particles. J Virol. American Society for Microbiology; 2004 Jul 15;78(14):7344–7351. PMCID: pmc434112

31. Ilinykh PA, Lubaki NM, Widen SG, Renn LA, Theisen TC, Rabin RL, Wood TG, Bukreyev A. Different Temporal Effects of Ebola Virus VP35 and VP24 Proteins on Global Gene Expression in Human Dendritic Cells. J Virol. 2015 Aug;89(15):7567–7583. PMCID: PMC4505630

32. Sugita Y, Matsunami H, Kawaoka Y, Noda T, Wolf M. Cryo-EM structure of the Ebola virus nucleoprotein–RNA complex at 3.6 Å resolution [Internet]. Nature. 2018. p. 137–140. Available from: http://dx.doi.org/10.1038/s41586-018-0630-0

33. Halfmann P, Kim JH, Ebihara H, Noda T, Neumann G, Feldmann H, Kawaoka Y. Generation of biologically contained Ebola viruses. Proc Natl Acad Sci U S A. 2008 Jan 29;105(4):1129–1133. PMCID: PMC2234103

34. Ebola vaccine (delta VP30) FAQ [Internet]. Waisman Center. 2018 [cited 2023 Oct 10]. Available from: https://www.waisman.wisc.edu/documents/ebola-vaccine-delta-vp30-faq/

35. Hume AJ, Mühlberger E. Distinct Genome Replication and Transcription Strategies within the Growing Filovirus Family. J Mol Biol. 2019 Oct 4;431(21):4290–4320. PMCID:

bioRxiv preprint doi: https://doi.org/10.1101/2023.12.01.569666; this version posted December 2, 2023. The copyright holder for this preprint (which was not certified by peer review) is the author/funder, who has granted bioRxiv a license to display the preprint in perpetuity. It is made available under aCC-BY-NC-ND 4.0 International license.

PMC6879820

36. Booth TF, Rabb MJ, Beniac DR. How do filovirus filaments bend without breaking? Trends Microbiol. 2013 Nov;21(11):583–593. PMID: 24011860

37. Miyake T, Farley CM, Neubauer BE, Beddow TP, Hoenen T, Engel DA. Ebola virus inclusion body formation and RNA synthesis are controlled by a novel domain of nucleoprotein interacting with VP35. J Virol [Internet]. American Society for Microbiology; 2020 Jul 30;94(16). Available from: https://journals.asm.org/doi/10.1128/JVI.02100-19 PMCID: PMC7394894

38. Jain S, Martynova E, Rizvanov A, Khaiboullina S, Baranwal M. Structural and Functional Aspects of Ebola Virus Proteins. Pathogens [Internet]. 2021 Oct 15;10(10). Available from: http://dx.doi.org/10.3390/pathogens10101330 PMCID: PMC8538763

39. Karlin S, Brocchieri L. Evolutionary conservation of RecA genes in relation to protein structure and function. J Bacteriol. 1996 Apr;178(7):1881–1894. PMCID: PMC177882

40. Livingstone CD, Barton GJ. Protein sequence alignments: a strategy for the hierarchical analysis of residue conservation. Comput Appl Biosci. 1993 Dec;9(6):745–756. PMID: 8143162

41. Valdar WS, Thornton JM. Protein-protein interfaces: analysis of amino acid conservation in homodimers. Proteins. 2001 Jan 1;42(1):108–124. PMID: 11093265

42. Dziubańska PJ, Derewenda U, Ellena JF, Engel DA, Derewenda ZS. The structure of the C-terminal domain of the Zaire ebolavirus nucleoprotein. Acta Crystallogr D Biol Crystallogr. 2014 Sep;70(Pt 9):2420–2429. PMCID: PMC4157450

43. Kirchdoerfer RN, Moyer CL, Abelson DM, Saphire EO. The Ebola Virus VP30-NP Interaction Is a Regulator of Viral RNA Synthesis. PLoS Pathog. 2016 Oct;12(10):e1005937. PMCID: PMC5068707

44. Xu W, Luthra P, Wu C, Batra J, Leung DW, Basler CF, Amarasinghe GK. Ebola virus VP30 and nucleoprotein interactions modulate viral RNA synthesis [Internet]. Nature Communications. 2017. Available from: http://dx.doi.org/10.1038/ncomms15576